Proteotype profiling unmasks a viral signaling network essential for poxvirus assembly and transcriptional competence

Karel Novy[1,6,7,¶], Samuel Kilcher[2,¶], Ulrich Omasits[1,6,7], Christopher Karl Ernst Bleck[3], Corina Beerli[2], Jakob Vowinckel[4], Caroline K. Martin[2], Mohammedyaseen Syedbasha[5], Alessio Maiolica[1], Ian White[2], Jason Mercer[2,*] & Bernd Wollscheid[1,6,7,*]

1 Institute of Molecular Systems Biology, D-BIOL, ETH Zurich, 8093 Zurich, Switzerland

2 MRC-Laboratory for Molecular Cell Biology, University College London, London WC1E 6BT, United Kingdom

3 Center for Cellular Imaging and NanoAnalytics (C-CINA), Biozentrum, University of Basel, 4058 Basel, Switzerland

4 Biognosys AG, Wagistrasse 21, 8952 Schlieren, Switzerland

5 Institute of Biochemistry, D-BIOL, ETH Zurich, 8093 Zurich, Switzerland

6 Biomedical Proteomics Platform, D-HEST, ETH Zurich, 8093 Zurich, Switzerland

7 Department of Health Sciences and Technology (D-HEST), ETH Zurich, 8093 Zurich, Switzerland

¶ These authors contributed equally to this work.

*Corresponding authors

E-Mail: jason.mercer@ucl.ac.uk (JM), wbernd@ethz.ch (BW)

Abstract

To orchestrate context-dependent signaling programs poxviruses encode two dual-specificity enzymes, the F10 kinase and the H1 phosphatase. These signaling mediators are essential for poxvirus production, yet their substrate profiles and systems level functions remain enigmatic. Using a phosphoproteomic screen of cells infected with wildtype, F10, and H1 mutant vaccinia viruses we systematically defined the viral signaling network controlled by these enzymes. Quantitative cross-comparison revealed 33 F10 and/or H1 phosphosites within 17 viral proteins. Using this proteotype dataset to inform genotype-phenotype relationships we found that H1-deficient virions harbor a hidden hyper-cleavage phenotype driven by reversible phosphorylation of the virus protease I7 (S134). Quantitative phosphoproteomic profiling further revealed that the phosphorylation-dependent activity of the viral early transcription factor, A7 (Y367), underlies the transcription-deficient phenotype of H1 mutant virions. Together these results highlight the utility of combining quantitative proteotype screens with mutant viruses to uncover proteotype-phenotype-genotype relationships that are masked by classical genetic studies.

Keywords: Vaccinia virus/ Proteotype analysis/ Phosphorylation / Signaling / Virus Maturation

Introduction

As a reversible post-translational modification, phosphorylation is indispensable for many fundamental cellular processes. It has become increasingly clear that dynamic phosphorylation also serves to regulate the replicative cycle of many viruses[1–3]. Advances in quantitative mass spectrometry based phosphoproteomic technology enable the interrogation of complex signaling programs, including viral phosphorylation networks[4–7]. Yet for most, a systems level understanding of viral phospho-networks and how they drive infection phenotypes and assure virion infectivity is lacking. Filling this gap in our knowledge of viral signaling networks provides an opportunity to bridge our current understanding of genotype-phenotype relationships using proteotype information.

Vaccinia virus (VACV) is the prototypic member of the *Poxviridae*, a family of large dsDNA viruses that include variola virus, the causative agent of smallpox[8]. Poxviruses, the largest, most complex mammalian viruses producing infectious mature virions (MVs) containing ~80 different viral proteins[9,10]. Assembly of these virions occurs exclusively in the cytoplasm of infected cells proceeding through several morphologically distinct stages reviewed elsewhere[8,11].

VACV encodes a set of enzymes to assure that assembly of these complex particles occurs in a tightly coordinated spatio-temporal fashion. These include the F10 kinase, two proteases (I7 and G1), a virus-encoded redox-system (E10, A2.5, G4), and the H1 phosphatase[11]. Classical genetic studies of inducible or temperature sensitive (*ts*) viruses show that each is essential for formation of infectious MVs[12–21]. The F10 kinase

is required for the earliest stage of morphogenesis, diversion of cellular membranes, I7 protease for the transition from immature virions (IVs) to MVs, and the H1 phosphatase assures virion transcriptional competence[14,18,22]. Although F10 and H1 share viral substrates important for virion assembly[11,23–25], the dynamic phospho-signaling network through which they regulate phosphorylation of viral proteins to drive production of infectious virions has not been evaluated.

Using quantitative mass spectrometry (MS)-based proteomics we dissected the abundance and phosphorylation status of proteins within VACV virions and the phospho-signaling network in cells infected with wild type (WT), F10 kinase-, and H1 phosphatase- deficient viruses. Comparison of these viral phospho-proteomes revealed 105 phosphosites in 43 viral proteins, 33 of which relied on F10 and/or H1. Analysis of I7 protease, a new F10/H1 substrate, indicated that dynamic phosphorylation at S134 drives virion structural protein cleavage. Relative quantitative comparison of phosphosites within WT and H1-deficient virions revealed that phosphorylation of the viral transcription factor A7 at Y367 directly contributes to the transcriptional incompetence of H1-deficient virions. These results establish a key role for dynamic phosphorylation in the regulation of infectious poxvirus particle assembly and highlight the utility of combining quantitative proteomic screens with mutant viruses to uncover proteotype-phenotype-genotype relationships.

Results

Defining the F10/H1 phosphoproteome

To define the viral phospho-signaling network regulated by the F10 kinase and H1 phosphatase we infected HeLa cells with either VACV WT, inducible F10 [vF10V5i referred to as F10(-)] or H1 [v*ind*H1 referred as H1(-)] recombinants under non-permissive condition[22,26] (Fig. 1A). Cells were harvested 12 hours post infection (h p.i.), when intermediate and late viral genes are maximally expressed[8,27]. Proteins were subjected to tryptic digestion and phosphopeptide enrichment on TiO_2 beads, resulting in phosphopeptide enrichments ranging between 71% and 84% (Supplementary Fig. 1A)

Samples were analyzed by data-dependent acquisition (DDA) LC-MS/MS and quantified across conditions. We identified 105 non-redundant serine (S), threonine (T), and tyrosine (Y) phosphorylation sites in 43 viral proteins (Supplementary Table 1). Relative quantification of the WT, H1(-), and F10(-) phospho-enriched samples revealed 28 unique F10-dependent phosphosites in 14 viral proteins, 21 unique H1-dependent phosphosites in 13 viral proteins, and 16 unique phosphorylation sites in 10 viral proteins regulated in an F10/H1 dependent fashion (Fig. 1B; green and purple boxes). Amongst the 10 shared substrates, 8 phosphosites were within 4 known shared substrates: S85 of A14, S235 of A4, S32, S167 and S197 of A17, and S229 and S261 of G7[11,22,23,28,29], and 8 phosphosites within 6 unknown shared substrates: A12, A19, G3, H5, F17, and I7. Amongst the F10/H1 substrates, two membrane proteins (A14, A17), 5 core proteins (A19, A4, A12, G7, H5), the lateral body protein F17, and the I7 protease, are essential for VACV assembly[11].

Proteotype profiling of phosphatase-deficient VACV virions

Often, phenotypic outcomes are best described by the underlying proteotype; the acute state of the proteome under given constraints[30]. We detected many quantitative changes in the VACV phosphoproteome in infected cells lacking F10 or H1 (Fig. 1B). To determine if these changes affected the virion proteotype at the level of protein abundance WT and H1(-) MVs were subjected to comparative proteomics. As F10 is essential for VACV morphogenesis, virions cannot be produced in its absence[13]. We identified and quantified 139 viral proteins between WT and H1(-) MVs (Fig. 1C, Supplementary Table 2). Forty-eight were less abundant by more than twofold in H1(-) MVs, including H1 which was down 43-fold. In line with previous reports[22], MV specific proteins A25 and A26 did not change abundance between WT and H1(-) MVs (Fig. 1C, dashed underlined label)[31], indicating no defect in MV production. As the majority of virions produced are MVs[8] and no striking changes in protein abundance between WT and H1(-) were seen, we reason that the F10/H1 phospho-signaling network doesn't control protein copy number for progeny virion assembly.

We next compared the phospho-proteotype of WT and H1(-) MVs. Quantitative phosphoproteomics analysis after TiO2 phosphopeptide enrichment (Supplementary Fig. 1A) yielded 179 phosphosites (78.6% serine and 21.4% threonine) on 47 viral proteins (Fig. 1D). Of these 179, 62 were hyperphosphorylated and 37 hypophosphorylated in H1(-) MVs (Fig. 1D, Supplementary Table 3). Of the 17 viral phosphoproteins comprising the F10/H1 phospho-signaling network in infected cells (Fig. 1B, Supplementary Table 1), only G3L was non-phosphorylated in MVs (Fig. 1D, Supplementary Table 3). Among the 21 H1 phosphosites identified in cells (Fig. 1B, purple squares), 15 were

hyperphosphorylated in H1(-) MVs. Of note, F10 and I7 protease, enzymes essential for MV formation, were identified as H1 substrates (Fig. 1B and 1D).

Dynamic phosphorylation of I7 is required for proteolytic processing and virus production

That F10 and I7 are H1 substrates suggested that in addition to assuring transcriptional competence of newly formed virions, H1 may facilitate their formation. Phosphorylation of F10 S7/8 or Y11 was recently reported, yet any link to H1 and the importance of these modifications was not investigated[32]. For this, we complemented an F10 mutant virus (*Cts*28) with F10-HA or F10-HA phosphomimetic and phosphodeletion mutants. These proteins rescued virus yield equally, suggesting that dynamic phosphorylation of F10 plays no role in virus assembly (Supplementary Fig. 2A and 2B).

Next we investigated the I7 protease, the enzyme essential for virion maturation via cleavage of core and membrane proteins[14,18,33]. Phosphoproteomics indicated that I7 S134 is phospho-regulated in an F10/H1-dependent fashion (Fig. 1B). To test if dynamic phosphorylation of S134 regulates I7 activity we used transient complementation of a VACV temperature-sensitive (*ts*) mutant of I7*, Cts16*[15,34]. This virus displays a 4'000-fold reduction in 24 h virus yield when grown at non-permissive temperature (40.0 °C). While virus production was complemented by 2-logs using a HA-tagged version of WT I7 (I7-HA), neither the phosphodeletion- (I7-HA S134A), nor the phosphomimetic- (I7-HA S134E) mutant could rescue virus yield (Fig. 2A). Immunoblot analysis assured that comparable amounts of WT and mutant proteins were expressed (Fig. 2A; inset). Next, cleavage of I7 core (p4a) and membrane (A17) substrates was analyzed[15,18]. While

expression of WT I7-HA rescued cleavage of both p4a and A17, I7-HA S134A and S134E mutants were unable to complement (Fig. 2B), strongly suggesting that F10/H1 dynamic phosphorylation of I7 at S134 is required for its protease activity.

F10 regulates I7 protease activity during the IV to MV transition

F10 is required for two stages of virus assembly; first for the diversion/formation of viral membranes[13,35], and second during the formation of IVs[36]. As we identified I7 as an F10 substrate (Fig. 1B), it reasoned that F10 may be required for I7-mediated proteolytic processing of viral proteins during IV formation. To assess if loss of F10 impacts I7-mediated proteolytic processing of viral proteins we used a rifampicin (Rif)-release assay to bypass the first F10-dependent stage of infection. Cells were infected with WT, or *ts*F10 viruses (*Cts15* or *Cts28*) in the presence of Rif at permissive temperature (31.0 ^{o}C) for 12 h, then released from RIF and kept at 31.0 ^{o}C or shifted to non-permissive temperature (40.0 °C) for 12 h (Fig. 2C). When released at 40.0 °C, *Cts15* and *Cts28* displayed a 48- and 400-fold decrease in virus yield, confirming the second F10-dependent block (Supplementary Fig. 2C). Analysis of p4a in *Cts15* and *Cts28* infected cells after Rif-release showed that at 31.0 ^{o}C p4a proteolytic processing occurred normally, while at 40.0 °C p4a remained unprocessed (Fig. 2D). These results suggest that I7 protease activity during IV formation and/or IV to MV maturation requires F10 kinase.

To gain spatial-temporal information of I7 S134 phosphorylation during morphogenesis we coupled the Rif-release with phosphoproteomics. WT infections were synchronized for 12 h in Rif and harvested or released from Rif for 10 min, 90 min, or 180 min.

Representative transmission electron microscopy (TEM) images confirmed the Rif block, many virosomes surrounded by flaccid membranes, and the synchronous resumption of viral morphogenesis upon its release (Fig. 3A; Rif). As reported[37,38], 10 min postrelease viral crescents appeared at the edge of the virosomes (Fig. 3A; T10). While at later times synchronization was less apparent, by 90 min IVs and IVs containing nucleoids (IVNs) were seen (Fig. 3A; T90). At 180 min postrelease vast numbers of mature virions had formed (Fig. 3A; T180).

Phosphoproteomics was employed to monitor I7 S134 phosphorylation. Prior to phosphoenrichment, crude heavy labeled tryptic peptides representing both phosphorylated and non-phosphorylated forms of I7 S134 were added to the trypsin digested samples at a constant concentration. Input samples and phospho-enriched samples were measured by LC-MS/MS using data independent acquisition (DIA). Phosphoenrichment was reproducible across samples (91.1 % to 96.8%; Supplementary Fig. 1B), enabling unbiased parallel monitoring of endogenous (light) and spiked-in (heavy) peptides. Co-elution of light and heavy forms of the AIDFpSQMDLK peptide at precursor- and fragment ion levels confirmed phosphorylation of I7 S134 (Supplementary Fig. 3A and 3B). In the presence of Rif significant phosphorylation of I7 was detected, as seen with other F10 substrates[23] (Fig. 3B). Within 10 min of Rif release I7 was rapidly dephosphorylated. At 90- and 180- postrelease I7 S134 phosphorylation increased over time reaching the level observed in the presence of Rif (Fig 3B; T90 and T180).

This suggests that I7 may be active during two stages of VACV morphogenesis, early during initial viral membrane formation and late during the IV to MV transition. Consistent with this, in the presence of Rif I7-mediated cleavage of membrane, but not core, proteins occurs[18,39]. To determine if there was a temporal correlation between I7 S134 phosphorylation and I7 activity, proteolytic processing of A17 and p4a during Rif release was assessed. In the presence of Rif A17 was cleaved and p4a was not (Fig. 3C; Rif). While A17 cleavage remained stable over the time course of Rif release, increasing only at T180, p4a cleavage was only observed at T180 postrelease (Fig. 3C; T180). As cleavage of A17 occurs on the virion surface and p4a cleavage within virions, it reasons that these results indicate that F10-mediated phosphorylation of I7 S134 regulates its proteolytic activity both temporally and spatially during VACV infection.

H1 regulates virion associated I7 proteolytic activity

As our data suggests that F10 phosphorylation activates I7, we reasoned that H1-mediated dephosphorylation may lead to I7 inactivation. To test if H1 regulates I7 activity, cells infected with H1(-) in the absence or presence of inducer (-/+ IPTG) were assessed for p4a cleavage over time (Fig. 4A). No major difference in p4a cleavage kinetics or efficiency was detected between the two conditions.

However, our Rif-release DIA data (Fig. 3C and D) indicated that I7-mediated p4a cleavage occurs within virions during the IV to MV transition[14,18]. In addition, the abundance of I7 and its core substrates remained unchanged between WT and H1(-) MVs (Fig. 1C), while phosphorylation of I7 S134 within H1(-) virions increased by 35-fold (Fig. 1D). Thus, we performed a quantitative comparison of I7 substrate peptide

distribution between WT and H1(-) MVs. In addition to p4a and A17, 4 core proteins: p4b (A3), G7, A12, and L4, undergo I7-mediated processing at conserved AG↓X motifs[18,23,40–44]. Single and consecutive tryptic peptides in the majority of I7 substrates showed significant abundance changes between WT and H1(-) MVs (Fig. 4B). Each of these localized to the AG↓X cleavage sites in the various proteins (Fig. 4B; red arrows). With the exception of G7, all polypeptides from regions of expected cleavage were less abundant in H1(-) MVs: For p4a the polypeptide between cleavage sites at positions 614 and 697 was down 2.5-fold, for p4b three consecutive polypeptides covering the N-terminus cleavage site at position 61 were 8.5-fold down, and for A12 the polypeptide containing the cleavage site at residue 56 was 3-fold down. For G7, one polypeptide harboring the second cleavage site at position 238 was 2.3-fold down while four consecutive polypeptides including the first cleavage site at position 187 were 1.7-fold more abundant. We could not assess L4 cleavage as the N-terminal cleavage site is upstream of the first tryptic cleavage site. For A17, two of three polypeptides harboring the cleavage sites at positions 16 and 185 were 4-fold and 3-fold less abundant in H1(-) MVs. Cleavage of A17 at position 16 releases the IV scaffolding protein D13 during the IV to MV transition[45–47]. Consistent with N-terminal hypercleavage of A17 in H1(-) virions, D13 was 5.8-fold less abundant in these MVs (Fig. 1C). Immunoblot analyses of p4a, p4b, and A17 in purified WT and H1(-) virions showed that cleavage is driven to completion in the absence of H1 (Fig. 4C). To assess if hypercleavage correlated with virion structural changes, cytoplasmic H1(-) and H1(+) virions were compared by TEM. No obvious morphological differences were detected between the two (Supplementary Fig. 4). Thus we show that in the absence of H1 phosphatase, virion associated I7 is hyperphosphorylated resulting in complete processing of I7 substrates. These results

further support an essential role for F10/H1 dynamic phosphorylation in the spatial/temporal control of I7 proteolytic activity.

Viral early transcription proteins are hyperphosphorylated in H1(-) virions

We next asked if we could use virion proteotype profiling to define the underlying cause of a mutant phenotype. While the phenotype of H1(-) virus is the production of transcriptionally incompetent virions[22], molecular understanding of this phenotype remains undefined. Comparison of WT and H1(-) MV proteomes showed no quantitative differences in the composition or abundance of viral transcription machinery (Fig. 1C, green and purple dots). In addition, no transcription proteins containing AG↓X sites were cleaved in H1(-) MVs (Supplementary Fig. 5), few were phosphorylated on serine/threonine, and none subject to H1 regulation (Fig. 1D, Supplementary Table 3). As H1 is a dual specificity enzyme[22,24], we analyzed tyrosine phosphorylation in WT and H1(-) virions[24,25,32]. For this, 5 mg of virions were purified and phosphotyrosine-containing peptides enriched by immunoprecipitation followed by LC-MS-MS. We identified and quantified 29 phosphotyrosines on 18 viral proteins within WT and H1(-) MVs (Fig. 5A). Amongst these, 3 components of the viral early transcription machinery were more phosphorylated in H1(-) virions: L3 on Y89/Y90, the RNA helicase NPH-II (I8) on Y634, and the viral early transcription factor (VETF) subunit A7 on Y367 (Fig. 5A; red bars, Supplementary Table 4)[48–52].

Dynamic phosphorylation of A7 is required for infectious virus formation

The identification of H1-regulated phosphotyrosines on viral transcription proteins provided a possible link between the proteotype and transcription-deficient phenotype of H1(-) MVs[22]. To address their functional relevance WT HA-tagged versions of L3, I8, and A7, and their corresponding phospho-deletion and phospho-mimetic mutants, were tested for complementation of non-permissive infections with inducible or *ts* viruses of each protein. For L3, the L3-HA was expressed but could not complement infectious virus production in non-permissive vL3Li-infected cells[36] (Supplementary Fig. 6A and 6B). For I8, the WT (I8-HA), phosphodeletion (I8-HA Y634A), and phosphomimetic (I8-HA Y367E) each expressed and rescued non-permissive *Cts*10 infection in correlation with the expression level of the complementing protein (Supplementary Fig. 6C and 6D). Transient complementation of non-permissive viA7 infections[53] showed that WT A7-HA was expressed and could rescue infection by 2-logs (Fig. 5B; pBSIIK A7-HA -dox). However, both phosphodeletion (A7-HA Y367A) and phosphomimetic (A7-HA Y367E) mutants failed to complement despite being expressed as well as WT A7-HA (Fig. 5B). These results suggest that dynamic phosphorylation of A7 Y367 is required for A7 function and infectious virus production.

A7 phosphomutants phenocopy transcription deficient H1(-) virions

Assuming the transcriptional defect in H1(-) virions is due to unregulated dynamic phosphorylation of A7, then A7 phosphomutants should phenocopy the H1(-) small plaque phenotype linked to their transcription defect[22]. Plaques formed by virions produced during transient complementation by A7-HA were indistinguishable from WT plaques (Fig. 5C; pBSIIKS A7-HA). Virions produced during transient complementation

with the phosphodeletion (A7-HA Y367A) or phosphomimetic (A7-HA Y367E) mutants produced few WT size plaques (Fig. 5B), and large numbers of tiny plaques reminiscent of those seen upon repression of H1 (Fig. 5C). We reasoned that the altered phosphorylation of A7 in these virions results in a transcriptional defect, rather than the assembly defect seen upon total loss of A7[50,53,54]. To differentiate these phenotypes we constructed viA7L mCherry-A4, an inducible A7 virus containing a fluorescent core, and expressing gpt-EGFP from an early-late promoter[53]. viA7L mCherry-A4 infected cells were transfected with A7-HA or the Y367A or Y367E A7 mutants and analyzed for MV formation (Fig. 5D). In the absence of inducer no discernable virion structures were formed (Fig. 5D; pBSIIKS - dox). When A7 was expressed, distinct mCherry-A4 punctae, were seen (Fig. 5D; pBSIIKS + dox). Transient expression of A7-HA, A7-HA Y367A, or A7-HA Y367E resulted in the formation of mCherry-A4 punctae indistinguishable from those in the presence of inducer (Fig. 5D). This suggested that the A7 phosphomutants could bypass the morphogenesis block seen upon A7 repression. To assure that these punctae correspond to MVs, A7 transient complementation experiments were analyzed by TEM. (Fig. 6A). During viA7L infections in the absence of inducer crescents and empty IVs were formed, while in the presence of inducer MVs were detected (Fig. 6A pBSIIKS + dox). In cells transiently expressing A7-HA, A7-HA Y367A, or A7-HA Y367E abundant MVs were observed (Fig. 6A). Quantification showed that MV formation in cells expressing WT or phosphomutant versions of A7 was comparable to that seen in the presence of inducer (Fig. 6B).

Discussion

Recent phosphoproteomic studies suggest that viruses, similar to eukaryotic cells, use phosphorylation to modulate protein function[32,57,58]. Their relative simplicity, lack of

redundancy, and genetic manipulability, make viruses outstanding tools to probe proteotype-phenotype-genotype relationships.

Revealing the F10/H1 viral signaling network

In vitro experiments on intravirion phosphorylation of VACV during activation/uncoating have been described[32,59]. These studies reported 29 phosphosites on 13 viral proteins modified by “intravirion kinases”. Of the 28 sites in 14 viral proteins we identified as F10 substrates (Fig. 1B), A14 (S85 and S88), A19 (S36 and S42), F10 (S7/S8/Y10), and G7 (T304/S305/T308/T312) were identified in these studies[32,59]. The modest overlap between phosphorylation events seen during MV uncoating/activation and virion morphogenesis supports the concept that dynamic phosphorylation regulates the virus lifecycle.

Focusing on the F10/H1 signaling network using proteomic profiling and mutant viruses we uncovered the largest intrinsic virus signaling network to date. Consistent with other studies[32,59] sequence alignment of 15 unambiguous sites provided no consensus for F10/H1 substrate recognition (Supplementary Fig. 7), suggesting that other features are required. None-the-less we uncovered 21 H1-dependent phosphosites within 13 substrates required for virion membrane assembly, maturation, and proteolytic processing (Supplementary Table 1). Highlighting the power of proteotype analyses, these results show that the F10/H1 signaling network regulates aspects of the VACV lifecycle beyond those revealed by mutant viruses.

Dynamic phosphorylation of I7 and VACV maturation

The phenotype of recombinant virus mutants always reflects the first temporal block in the virus lifecycle. This makes it nearly impossible to define additional phenotypes that underlie the loss of a particular protein. Using quantitative phosphoproteomics of WT, F10(-) and H1(-) infected cell lysates we show that the viral protease I7 is a F10/H1 substrate and demonstrate a genetic link between F10 and I7 proteolytic activity. Using phosphoproteomics with spike-in of heavy labeled reference peptides in combination with DIA mass spectrometry, we further show that F10-mediated phosphorylation of I7 S134 occurs during two independent stages of infection: early during viral membrane diversion, and late during IV formation/IV to MV transition. That early I7 proteolytic activity correlated with extravirion cleavage of A17 and late activity with cleavage of p4a within the virion suggested that F10-dependent I7 activity was also spatially regulated. Corroborating this notion, proteotype profiling uncovered an I7 substrate hypercleavage phenotype within H1(-) virions. That this phenotype was detected in purified virions but not infected cell lysates dictates that regulation of I7-mediated core protein processing occurs within virions. Together, these results indicate that I7 proteolytic activity is controlled by F10/H1 dynamic phosphorylation in a spatial/temporal fashion. Perhaps the differential sub-virion localization of F10[16] and H1[61] reflects the need to partition their activities for successful I7 mediated virion maturation.

H1(-) MV proteotype and transcriptional defect

Phosphoproteotype analysis of virion associated transcription machinery revealed that three early transcription proteins displayed increased tyrosine phosphorylation in H1(-) MVs (Fig. 5A and Supplementary Table 4). Of these, dynamic phosphorylation of A7 Y367 was required for productive virus infection (Fig. 5B). While complete repression of

A7 results in an assembly defect[53,55,56], targeted mutation of Y367 allowed for the formation of MVs. That these virions phenocopy H1(-) virions[22], suggests that the transcription deficiency of H1(-) is due, at least in part, to hyperphosphorylation of A7. Within MVs A7 is located inside the core and H1 relegated to LBs[61]. This would suggest that virion transcriptional competence must be assured in IVs when H1, A7, and other early transcription factors are within a single virion compartment (Fig. 6C).

Our results reveal the underlying complexity and implicit spatial/temporal regulation of the F10/H1 signaling network required to assure the formation of infectious poxvirus particles. By combining mutant viruses and proteotype profiling we have demonstrated that one can go beyond virus genotype-phenotype relationships to define viral signaling networks, uncover masked phenotypes, and define new links between mutant virus phenotypes and their causal proteotypes.

Experimental Procedures

Antibodies and drugs

Mouse anti-HA MAb HA.11 (16B12) was purchased from Covance (Princeton, NJ, USA). Mouse anti-α-tubulin MAb DM1A and mouse anti-γ-tubulin MAb GTU-88 were purchased from Sigma-Aldrich (St. Louis, MO, USA). Rabbit anti-α-tubulin MAb (11H10) was purchased from Cell Signaling Technologies (Danvers, MA, USA). Anti-4a was generously provided by Dr. Dennis E. Hruby (Oregon State University). Anti-A17 and anti-A4 were generously provided by Dr. Jacomine Krijnse-Locker (Institute Pasteur).

Goat anti-mouse AlexaFluor® 647 conjugated secondary antibody was purchased from Life Technologies. Rifampicin, doxycycline hyclate, and isopropyl β-D-1-thiogalactopyranoside (IPTG) were purchased from Sigma-Aldrich.

Cell and viruses

African green monkey BSC-40 cells (ATCC CRL-2761) and HeLa cells (ATCC CCL2) used throughout this study were not independently authenticated in our laboratories. Both cell lines were cultivated in DMEM (Life Technologies, Carlsbad, CA, USA) supplemented with 10% heat-inactivated FCS, sodium-pyruvate, non-essential amino acids, glutamax, and penicillin-streptomycin. Regular testing assured that cell lines used throughout this study were negative for mycoplasma contamination.

Temperature-sensitive VACV strains *Cts15* (F10L)*, Cts28* (F10L)*, Cts16* (I7L), and *Cts10* (I8R) were kindly provided by Dr. Richard Condit [34] (University of Florida, Gainesville, FL, USA) and grown at 31 °C. A doxycycline-inducible VACV mutant of the A7L gene (viA7L) was a kind gift of Dr. Paulo H. Verardi [53] (University of Connecticut, Mansfield, CT, USA). IPTG-inducible VACV strains of the F10L and L3R genes were kindly provided by Dr. Bernard Moss [26,51] (National Institutes of Health, Bethesda, MD, USA) and grown in the presence of 50 μM, and 25 μM IPTG, respectively. The IPTG-inducible VACV strain vindH1 was a kind gift of Paula Traktman[22] (Medical University of South Carolina, SC, USA) and grown in the presence of 5 mM, IPTG. Recombinant VACV strain viA7L mCherry-A4 was generated based on strain viA7L by replacing the endogenous A4L gene with the mCherry-A4L fusion as described before [62,63]. Recombinant viA7 mCherry-A4 was identified based on plaque fluorescence and purified by at least two rounds of plaque purification. MV particles were produced in BSC-40 cells and purified from cytoplasmic lysates as described elsewhere [64].

Lysis and tryptic digest

MVs or infected cells were vortexed for 10 min at full speed in 8 M urea containing 100 mM ammonium bicarbonate pH 8.2, one tablet of phosphatase inhibitors cocktail (PhosStop, Roche) per 10 mL buffer followed by three times sonication of 30 sec each at 80% amplitude and 0.8 cycle (Vialtweeter, Hielscher). The insoluble fraction was pelleted at 15,000 x g for 10 min and the supernatant was collected. The proteins were reduced with 5 mM tris(2-carboxyethyl)phosphine for 20 min at room temperature. Free cysteines were alkylated with 10 mM iodoacetamide for 30 min at room temperature in the dark. For tryptic digest, the solution was diluted eight fold with 100 mM ammonium bicarbonate pH 8.2 and sequence grade trypsin (Promega) was added to a protein:enzyme ratio of 50:1 and incubated for 16 hours at 37°C under constant agitation. Trypsin was inactivated by addition of trifluoroacetic acid (TFA) to a final concentration of 0.2% (v/v). Resulting peptides were desalted on a reverse phase C18 column (Waters) and eluted with 50% acetonitrile (ACN), 0.5% TFA. The solvents were evaporated using a centrifuge evaporator device. Peptides from MV origin (H1(-) or WT) were either resuspended in 2% ACN, 0.1% formic acid (FA) for direct LC-MS/MS analysis for whole proteome comparison or further processed as described below.

Heavy-labeled peptide synthesis

The internal standards used for relative quantification of I7 and I7 S134 phosphorylation were obtained from JPT Peptide Technology, Berlin, Germany. The peptide sequences AIDFSQMDLK and AIDFpSQMDLK were synthesized with a stable isotope standard label on the C-terminal lysine K (U-13C6;U-15N2). Crude synthetic peptides were resuspended in 0.2:0.8:0.1 ACN/H2O/TFA and further diluted with 1:0.1 H2O/TFA. A constant amount of AIDFSQMDLK peptide was spike into the protein digested samples

before C18 desalting and, in the case of the AIDFpSQMDLK peptide, before phosphopeptide enrichment.

Phosphopeptides enrichment on titanium dioxide beads

2 mg MVs or 3 mg proteins from infected HeLa CCL2 cells (~15 x 10^6 cells) were lysed and digested as described above. Biological triplicates were used for each condition. Phosphopeptide enrichment was adapted from[65]. 1.25 mg TiO_2 resin was used per 1 mg desalted peptides, (Titansphere, 5 micron, GL Sciences). The resin was washed with 2-propanol and incubated in saturated phtalic acid solution containing 80% ACN and 3.5% TFA. The peptides were solubilized in the same phtalic acid solution. The resin was added to the peptide solution, incubated for one hour at room temperature and pelleted. The supernatant was discarded, the resin washed twice with phtalic acid solution and three times with 50% ACN, 0.1% formic acid (FA). Bound peptides were eluted with 0.3 M ammonium hydroxide and acidified with TFA to pH <3. Subsequently the peptides were desalted using a C18-column (UltraMicroSpin, The Nest Group) following the manufacturer's instructions. Desalted peptides were dried in a centrifuge evaporator device and resuspended in 2% ACN, 0.1% FA for LC-MS/MS analysis.

Immunoprecipitation of peptides containing phosphorylated-tyrosine

Peptides containing phosphorylated tyrosine residue(s) were enriched following the instructions of the PTMScan Phospho-Tyrosine P-Tyr-100 kit (Cell Signaling Technology). Briefly, 5 mg of desalted peptides from MV lysate were resuspended in IAP buffer plus detergent and incubated with p-Tyr-100 antibodies coated beads. The beads were washed and eluted with 0.15% TFA according to the manufacturer instructions. Enriched peptides were desalted using C18 containing tips (ZipTip, Millipore). Desalted

peptides were dried in a centrifuge evaporator and resuspended in 2% ACN, 0.1% FA for LC-MS/MS analysis. Due to the high protein amount needed for pY enrichment, we restricted our analysis to one unique replicate for each condition [H1(-) or WT MVs].

Liquid Chromatography–Tandem Mass Spectrometry (LC-MS/MS)

Data-dependent acquisition (DDA)

Phosphopeptide enriched samples from MVs and HeLa cells were separated by reversed-phase chromatography on a high pressure liquid chromatography (HPLC) column (75 μm inner diameter, New Objective) that was packed in-house with a 10 cm stationary phase (Magic C18AQ, 200 Å, 3 Michrom Bioresources) and connected to a nano-flow HPLC combined with an autosampler (EASY-nLC II, Proxeon). The HPLC was coupled to a LTQ-Orbitrap XL mass spectrometer (Thermo Scientific) equipped with a nanoelectrospray ion source (Thermo Scientific). Peptides were loaded onto the column with 100% buffer A (99.9% H2O, 0.1% FA) and eluted at a constant flow rate of 300 nl/min over a 60 min (MVs) or a 90 min (HeLa) linear gradient from 7% to 35% buffer B (99.9% ACN, 0.1% FA). After the gradient, the column was washed with 80% buffer B and re-equilibrated with buffer A. Mass spectra were acquired in a data-dependent manner, with an automatic switch between MS and MS/MS scans. High-resolution MS scans were acquired in the Orbitrap (resolution 60,000 at 400 m/z, automatic gain control (AGC) target value 10^6 to monitor peptide ions in the mass range of 300–1,600 m/z, followed by collision-induced dissociation (CID) MS/MS scans in the ion trap (minimum signal threshold 250, AGC target value 10^4, isolation width 2 m/z) of the five most intense precursor ions. To avoid multiple scans of dominant ions, the precursor ion masses of scanned ions were dynamically excluded from MS/MS analysis

for 30 s. Singly charged ions and ions with unassigned charge states were excluded from MS/MS fragmentation.

Peptide samples from whole MV lysis were separated by reversed-phase chromatography on an ultra high pressure liquid chromatography (uHPLC) column (75 µm inner diameter, 15 cm, C18, 100Å, 1.9 µm, Dr. Maisch, packed in-house) and connected to a nano-flow uHPLC combined with an autosampler (EASY-nLC 1000, Thermo Scientific). The uHPLC was coupled to a Q-Exactive Plus mass spectrometer (Thermo Scientific) equipped with a nanoelectrospray ion source (NanoFlex, Thermo Scientific). Peptides were loaded onto the column with buffer A (99.9% H_2O, 0.1% FA) and eluted at a constant flow rate of 300 nl/min over a 90 min linear gradient from 7% to 35% buffer B (99.9% ACN, 0.1% FA). After the gradient, the column was washed with 80% buffer B and re-equilibrated with buffer A. Mass spectra were acquired in a data-dependent manner, with an automatic switch between MS and and MS/MS scans. Survey scans were acquired (70,000 resolution at 200 m/z, AGC target value 10^6) to monitor peptide ions in the mass range of 350–1,500 m/z), followed by higher energy collisional dissociation (HCD) MS2 scans (17,500 resolution at 200m/z, minimum signal threshold 420, AGC target value $5x10^4$, isolation width 1.4 m/z) of the ten most intense precursor ions. To avoid multiple scans of dominant ions, the precursor ion masses of scanned ions were dynamically excluded from MS/MS analysis for 10 s. Singly charged ions and ions with unassigned charge states were excluded from MS/MS fragmentation.

Data independent acquisition (DIA)

Retention time peptides (iRT peptides, Biognosys AG, Switzerland) were added to the input (non-phosphoenriched peptide) and phosphopeptide samples from the Rif release time course experiment performed in HeLa cells. 1ug peptide of each sample was

loaded on the analytical column and separated by reversed-phase chromatography on an ultra high pressure liquid chromatography (uHPLC) column (75 µm inner diameter, 15 cm, C18, 100Å, 1.9 µm, Dr. Maisch, packed in-house) and connected to a nano-flow uHPLC combined with an autosampler (EASY-nLC 1000, Thermo Scientific). The uHPLC was coupled to either a Q-Exactive Plus (input sample) or a Fusion Tribrid mass spectrometer (phosphosamples) (both Thermo Scientific) equipped with a nanoelectrospray ion source (NanoFlex, Thermo Scientific). Peptides were loaded onto the column with buffer A (99.9% H_2O, 0.1% FA) and eluted at a constant flow rate of 300 nl/min over a 120 min linear gradient from 7% to 35% buffer B (99.9% ACN, 0.1% FA). After the gradient, the column was washed with 80% buffer B and re-equilibrated with buffer A. Survey scan covering the 400-1220 m/z range (MS1, 60'000 resolution, AGC target 1E6, 64ms), followed by higher energy collisional dissociation (HCD) mass spectra acquired in a data-independent (DIA) manner using 19 overlapping variable windows (MS2, 30'000 resolution, AGC target 1E6, injection time 54 ms).

VACV H1(-) and WT MV relative protein quantification

SEQUEST (v27.0)[66] was used to search fragment ion spectra for a match to fully tryptic peptides without missed cleavage sites from a protein database, which was composed of human proteins (SwissProt, v57.15), Vaccinia virus proteins (UniProt, strain Western Reserve, v57.15), various common contaminants, as well as sequence-reversed decoy proteins. The precursor ion mass tolerance was set to 20 ppm. Carbamidomethylation was set as a fixed modification on all cysteines. The PeptideProphet and the ProteinProphet tools of the Trans-Proteomic Pipeline (TPP v4.6.2) [67] were used for probabilistic scoring of peptide-spectrum matches and protein inference. Protein identifications were filtered to reach an estimated false-discovery rate of ≤1%. Peptide

feature intensities were extracted using the Progenesis LC-MS software v2.0 (Nonlinear Dynamics). Protein fold changes and their statistical significance between paired conditions were tested using at least two fully tryptic peptides per protein with the MSstats library (v1.0)[68]. Resulting p-values were corrected for multiple testing with Benjamini-Hochberg method[69].

Phosphorylation site identification and localization

SEQUEST (v27.0) [66] was used to search fragment ion spectra for a match to semi-tryptic peptides with up to two missed cleavage sites from a protein database, which was composed of human proteins (SwissProt, v57.15), Vaccinia virus proteins (UniProt, strain Western Reserve, v57.15)[70], various common contaminants, as well as sequence-reversed decoy proteins. The precursor ion mass tolerance was set to 0.05 Da. Carbamidomethylation was set as a fixed modification on all cysteines and phosphorylation of serines, threonines and tyrosines as well as oxidation of methionines was considered as optional modification. Resulting peptide-spectrum matches (PSMs) were statistically validated and filtered for a minimum probability of 0.9 using PeptideProphet (TPP v4.6.2)[67]. Phosphorylated PSMs were further assessed using PTMprophet (TPP v4.6.2)[71] computing a localization probability for any of the serines, threonines and tyrosines within a peptide sequence. Based on these probabilities we pinned down phosphorylations to actual sites as follows. For a PSM where a phosphorylation was localized to a site with a probability of 0.9 or higher, this site was considered phosphorylated. Phosphorylation sites with a probability of 0.1 or lower were discarded. For a PSM with phosphorylation localization probabilities between 0.1 and 0.9, the following heuristic was used to derive the phosphorylation site: For each phosphorylation site its maximum localization probability across all samples was

calculated. If there was only one site with a sample-wide probability of 0.9 or higher, this site was considered phosphorylated. If there were multiple sites with sample-wide probabilities of 0.9 or higher, those sites were combined to a “shared phosphorylation”. Also, if none of the sites had a sample-wide probabilities of 0.9 or higher, the sites were combined to a “shared phosphorylation” and reported with the separator “|”. This procedure was repeatedly applied for multiply phosphorylated PSMs.

Phosphorylation site quantification and differential expression analysis

Peptides were quantified on MS1 level using Skyline (version 1.3)[72]. The integrated areas of a peptide’s isotopic peaks were summed up and peptides with ambiguous PTM sites were merged if they had a retention time overlap of more than 50%. Phosphorylation site localization was determined as described above. MSstats (version 1.0)[68] was used to determine statistically significant differentially expressed phosphorylation sites by building an ANOVA model for each site, based on all quantified peptides featuring this site. Shared phosphorylation sites as well as protein groups were used in each site/group repeatedly. Tests for differential expression were performed for each site and each pair of conditions and resulting p-values were corrected for multiple testing with Benjamini-Hochberg method[69].

Data Analysis of DIA LC-MS/MS Experiment

LC-MS/MS DIA runs were analyzed with the software Spectronaut™ Pulsar version 11.0.18206.14.29112 (Biognosys AG, Switzerland) [73,74] using default settings. Briefly, a

spectral library for the input samples (non phospho-enriched) was generated from 4 input samples measured in DDA on a Q-Exactive HF (Thermo Scientific). DDA data were searched with MaxQuant[75,76] using a combined protein database human (SwissProt, v57.15) and Vaccinia virus (UniProt, strain Western Reserve, v57.15), full tryptic allowing two missed cleavages including carbamidomethylation as a fixed modification on all cysteines and oxidation of methionines and protein N-terminal acetylation as optional modifications. For the phosphoenriched samples, DIA runs were directly searched using the DirectDIA™ function of Spectronaut™ Pulsar [77], full tryptic allowing two missed cleavages including carbamidomethylation as a fixed modification on all cysteines, oxidation of methionines, protein N-terminal acetylation and phosphorylation of serines, threonines and tyrosines as optional modifications. Both spectral libraries were imputed with the mass spectrometric assays of the heavy labeled peptides spike-in which were derived in silico in Spectronaut Pulsar from the identified endogenous peptides. Spectral libraries were then used for targeted data extraction of DIA runs in Spectronaut Pulsar. Extracted peptide intensities were used for plotting in R.

Immunofluorescence and electron microscopy

BSC-40 cells were seeded onto 13 mm glass coverslips in 24-well plates, infected with strain viA7 mCherry-A4 at an MOI of 4 as described in the transient complementation section, and transfected with 800 ng plasmid and 3 ul Lipofectamine2000. For immunofluorescence staining, cells were fixed in 4% formaldehyde, permeabilized with 0.5% Triton X-100, and stained with primary anti-HA (1:1000) and AlexaFluor-647-coupled secondary antibody (1:1000). Images were acquired using a Leica DM2500 confocal microscope. For conventional TEM, coverslips were fixed in 2.5% glutaraldehyde (0.05 M sodium cacodylate adjusted to pH 7.2, 50 mM KCl, 2.5 mM

CaCl2) for 45 min at RT. After several washes with 50 mM sodium cacodylate buffer, they were postfixed in OsO4 (2% OsO4 in water) for 1 hr on ice, followed by blockstaining in 0.5% aqueous uranyl acetate overnight. The specimens were then dehydrated in graded ethanol series and propylene oxide, followed by embedding in Epon. Ultrathin sections (50-60 nm) were obtained using a FC7/UC7-ultramicrotome (Leica, Vienna, Austria). Sections were examined with a CM10 Philips transmission electron microscope with an Olympus “Veleta” 2k x 2k side-mounted TEM CCD camera.

Transient complementation assay

VACV genes F10L, I7L, L3R, I8R, and A7L and their endogenous promoters were amplified from VACV genomic DNA. C-terminal HA-tags were introduced by two consecutive rounds of PCR and the products cloned into pBSIIKS using the primers and enzymes listed in Supplementary Table 5. Amino acid changes were introduced using quickchange site-directed mutagenesis (Agilent Technologies, Santa Clara, CA, USA).

For transient complementations, confluent 6-well dishes of BSC-40 cells were infected at an MOI of 4 as for the Rif-release experiment and then maintained either at permissive / induced or non-permissive / non-induced condition, as indicated. At 4 h postinfection (p.i.), 4 ug of plasmid DNA encoding either the wild-type protein sequence or phosphodeletion and phosphomimetic mutations thereof were introduced by transfection using 15 ul Lipofectamine2000 reagent. Empty vector (pBSIIK) was used as control. At 24 h p.i., produced infectious virions were isolated as described and titered on BSC-40 cells at the permissive condition. For I8R transient complementations, cells were maintained at permissive condition until 5 h p.i. to allow early transcription of the thermolabile particle[78]. Expression of transfected constructs was verified by western blot (WB) analysis using anti-HA antibodies. Full immunoblot images of all cropped

immunoblots presented throughout the manuscript are presented in Figure S8.

Data availability

The datasets generated during and/or analysed during the current study are available in the MassIVE repository (http://massive.ucsd.edu/ MassIVE ID: MSV000081854.
Data can be downloaded via FTP: ftp://massive.ucsd.edu/MSV000081854. The DIA runs and spectral libraries can be reviewed with the Spectronaut Viewer software (www.biognosys.com/spectronaut-viewer).

Conflict of Interest Statement

Jakob Vowinckel is an employee of Biognosys AG and helped with the Spectronaut DIA analysis in the revised version of the manuscript. Karel Novy joined Biognosys AG during the revision process of the manuscript upon finishing his PhD at ETH Zurich.

All correspondence and/or requests for materials should be directed to Jason Mercer (jason.mercer@ucl.ac.uk) or Bernd Wollscheid (wbernd@ethz.ch)

Acknowledgments

We would like to thank Paula Traktman, Richard Condit, Bernard Moss, and Paulo H. Verardi for generously donating VACV mutants for this study. We greatly acknowledge Andreas Frei, Sandra Götze and Alexander Leitner for maintenance of the mass spectrometers. We are grateful to all members of the Mercer and Wollscheid labs for critical comments and suggestions throughout this project. This work was supported by the Swiss National Science Foundation (31003A_160259 to B.W.) and the InfectX

project from the Swiss Initiative in Systems Biology SystemsX.ch (to B.W.), MRC Programme Grant (MC_UU12018/7) (J.M.), the European Research Council (649101 UbiProPox) (J.M.), and Swiss National Foundation Ambizione; PZ00P3_131988 (J.M.).

Author Contributions

K.N., S.K., J.M. and B.W. designed the project and wrote the manuscript. K.N. performed the proteomic experiments. K.N., U.O. and J.V. analyzed the proteomics data and U.O. performed the phosphorylation site re-localization analysis. M.S. produced viruses. S.K., C.B. and C.K.M. designed and performed the biochemical validations. S.K, C.K.E.B. and I.W. performed the EM analysis. A.M. contributed ideas and assistance for the phosphoproteomic workflows. All authors discussed the results and implications of the findings and provided comments on the manuscript at all stages.

Figure Legends

Figure 1: Proteotype-based decoding of the viral signaling network. (A) Conceptual approach and analytical strategies adopted in this study to uncover the viral signaling network and its function (B) Heat map showing the relative abundance of viral phosphorylation sites (S, T, and Y) between VACV WT, F10(-), H1(-) infected cells and uninfected cells. The last column on the right (Reg.) indicates phosphosites regulated in an F10 (green square) and/or H1 (purple squares) dependent fashion by at least 2-fold relative to WT infections. Experiments were performed in biological triplicate and significance scored as a minimum of 2-fold with an adjusted p-value ≤ 0.05). (C) Relative abundance of viral proteins in WT versus H1(-) MVs. Proteins are color-coded as more abundant (red), less abundant (blue), or displaying no change in abundance (black) in

H1(-) MVs relative to WT MVs. Experiments were performed in biological triplicate and proteins displaying at least a 2-fold change in abundance (+/-) with an adjusted p-value ≤ 0.01 were considered significant. (D) Relative abundance of viral phosphorylation sites between H1(-) and WT MVs. Each phosphorylation site is labeled as the viral protein name and its amino acid position. Phosphosites are color-coded as more abundant (red), less abundant (blue), or displaying no change in abundance (black) in H1(-) MVs relative to WT MVs. Experiments were performed in biological triplicate. Only phosphorylation sites that change in abundance at least 2-fold (+/-) with an adjusted p-value ≤ 0.05 between H1(-) and WT MVs are considered significant.

Figure 2: F10 dependent phosphorylation of I7 modulates cleavage of viral structural proteins. (A) BSC40 cells were infected with *Cts16* (MOI=4), transfected with empty plasmid (pBSIIK) or the various I7-HA constructs, and infectious yields were determined at 24 h. Mean ± SEM is shown for 3 biological replicates. Immunoblot analysis using α-HA confirmed the expression of the various I7 proteins (inset). (B) proteolytic processing of the core protein P4a and the membrane protein A17 by transiently expressed I7 proteins at 40 °C was assessed by immunoblot analysis with immunoblot against tubulin serving as a loading control. (C) BSC40 cells were infected with VACV WT, Cts15, or Cts28 (MOI=4) for 12 h in the presence of Rif at 31°C. Cells were then washed and released into medium without Rif for 12 h at 31°C or 40 °C. (D) Following the protocol outlined in (C), cells lysates were analyzed for cleavage of the core structural protein P4a. Immunoblots directed against tubulin were used as loading control. All immunoblots are representative of 3 independent biological replicates.

Figure 3: Phosphorylation of I7 S134 is temporally regulated during virus

assembly. (A) HeLa cells were infected with VACV WT (MOI=5) for 12 h in the presence of Rif and subsequently released into medium without Rif for 10 m, 90 m or 180 m. Samples were prepared for epon embedding and conventional TEM. Morphogenesis intermediates formed in the presence of Rif or upon Rif-release are shown. Rifampicin bodies (RB); Crescents (C); Immature virions (IV); Immature virions with DNA nucleoids (IVN) and mature virions (MV) are labelled. Scale bars = 1µm. Representative images of from 2 biological replicates are shown. (B) Cells prepared as in (A) were subjected to HRM/DIA mass spectrometry with heavy labeled spike-in peptides for the relative quantitative assessment of both I7 and I7 S134 phosphorylation. The relative abundance of I7 and I7 S134 (normalized to 0 min) over time are displayed. Mean ± SEM is shown for 3 biological replicates. Statistical significance at $P<0.001$ (student's t-test) of I7 S134 phosphorylation changes between 0 min and 10 min and between 10 min and 180 min is displayed with an asterisk. (C) Cells lysates as prepared in (A) were analyzed for cleavage of the membrane protein A17 and the core structural protein P4a. Immunoblots directed against tubulin were used as loading control. Representative blots from 3 independent biological replicates.

Figure 4: H1 regulates virion-associated I7 proteolytic activity. (A) Time course of P4a cleavage in v*ind*H1 infected cell lysates in the absence (-) and presence (+) of inducer. (B) The relative change in abundance of tryptic peptides measured for structural proteins between H1(-) and WT MVs are displayed on the proteins' linear sequence from N- to the C- terminus. The protein name and percent sequence coverage obtained are displayed. Each bar represents a tryptic peptide, its width the amino acids covered, its height the relative abundance (up being more abundant and down being less abundant) between H1(-) and WT MVs. Experiments were performed in biological triplicate.

Peptides showing significant changes in abundance (≥ 1 fold up/down with an adjusted p-value ≤ 0.0001) are red, peptides showing no significant change in abundance are blue. Red arrows mark the positions of I7 cleavage sites at AG↓X consensus sequences. (C) Immunoblot analysis of showing the proteolytic processing of the core proteins P4a, P4b and the membrane protein A17 in purified MVs isolated from cells infected by either VACV WT or V*ind*H1 without addition of inducer with immunoblot against the core protein A4 serving as a loading control. All immunoblots are representative of 3 independent biological experiments.

Figure 5: Tyrosine phosphorylation of viral early transcription factor A7 controls virion transcription but not assembly. (A) Band-purified WT and H1(-) MVs were lysed in 8 M urea, digested with trypsin, phosphotyrosine containing peptides purified using anti-phosphotyrosine antibodies, and peptide abundance quantified by LC-MS/MS. The relative abundance of phosphorylated Y residues is shown for H1(-) versus WT MVs. Hyperphosphorylated early transcription proteins are highlighted in red. Data acquired on a single biological replicate (B) For transient complementation of viA7 infection, BSC-40 cells were infected with viA7 (MOI=4) in the absence (-dox) or presence (+dox) of inducer for 4 h prior to transfection with empty plasmid (pBSIIK), or A7-HA constructs. At 24 hours post infection samples were harvested and cell lysates analyzed by immunoblot for A7 expression (α-HA) and α-tubulin as a control (Inset). The infectious yields of the various transient complementation assays were determined by plaque assay. The means ± SEM of 3 biological replicates are displayed. (C) Plaque morphology seen upon transient complementation with the WT, phosphodeletion and phosphomimetic A7 mutants in the presence of doxycycline and at distinct dilution factor (DF). Representative images from 3 biological replicates are shown. (D) Transient

complementation of A7 virion morphogenesis defect with the WT, phosphodeletion and phosphomimetic A7 mutants. VACV viA7L mCherry-A4 MVs were bound to BSC-40 cells on glass-coverslips at RT (MOI=4). Samples were incubated for 4 h at 37°C and subsequently transfected with empty plasmid (pBSIIKS) or the various A7-HA constructs in presence or absence of doxycycline, as indicated. At 24 hours post infection the coverslips were fixed, permeabilized, and stained with α-HA antibodies to detect A7 expressing cells. Cells were then imaged for A7 expression (α-HA), infection (EL gpt-EGFP), and A4 positive virions (mCherry-A4). Representative confocal images from 3 biological replicates are shown. Gpt = xanthine-guanine phosphoribosyl transferase. Scale bar = 10 µm.

Figure 6. Intact MVs are formed in the absence of A7 Tyr phosphorylation exemplifying phosphodynamic regulation of poxvirus assembly by F10 and H1. (A) Transient complementation infection assays using viA7L were performed as in Figure 5. Samples were prepared for epon embedding and conventional TEM. Representative images (N=2) of the morphogenesis intermediates formed in the absence (pBSIIKS - dox) and intact virions in the presence (pBSIIKS + dox) of A7 expression, or transient complementation with A7 constructs. Regions of interest are boxed and magnified to the right of the micrographs. (B) For each sample the average number of mature virions per section was quantified. Non-transfected cells formed no MVs in the absence of doxycycline and were excluded from analysis (grey triangles). A minimum of 24 cells was quantified per condition (N=2). Scale bar = 1.5 µm. (C) Model of poxvirus assembly driven by F10 kinase and H1 phosphatase. Virion assembly begins with formation of viral crescents, which relies on F10 and membrane proteins A14 and A17, which are F10/H1 substrates. During this process, A17 is proteolytically processed by

phosphorylated I7. As crescents grow to form IVs they encapsidate virosomal material including, virus enzymes (F10, H1, and I7), core structural proteins (A4, A12, A19, H5, 4A, and 4B), and LB components (F17). During IV formation I7 phosphorylation is low, perhaps to prevent full cleavage of A17 and allow for recruitment of the D13 scaffold. Packaging of the viral genome and early transcriptional machinery, including A7, completes the formation of IVNs. During the IVN to MV transition I7 phosphorylation increases and the protease acts outside virions to cleave A17 and release D13, and within virions to process core components. Finally, to assure that the MVs formed are infectious, H1 dephosphorylates the early transcription factor A7 assuring MV transcriptional competence. Collectively, our data suggest that the formation of intact infectious MVs requires a delicate balance of spatial and temporal F10/H1-mediated phosphoregulation.

References

1. Biedenkopf, N., Lier, C. & Becker, S. Dynamic Phosphorylation of VP30 Is Essential for Ebola Virus Life Cycle. *J. Virol.* **90,** 4914–4925 (2016).
2. Mondal, A., Potts, G. K., Dawson, A. R., Coon, J. J. & Mehle, A. Phosphorylation at the homotypic interface regulates nucleoprotein oligomerization and assembly of the influenza virus replication machinery. *PLoS Pathog.* **11,** e1004826 (2015).
3. Zhao, X. *et al.* Phosphorylation of Beet black scorch virus coat protein by PKA is

required for assembly and stability of virus particles. *Sci. Rep.* **5,** 11585 (2015).

4. Sharma, K. *et al.* Ultradeep human phosphoproteome reveals a distinct regulatory nature of Tyr and Ser/Thr-based signaling. *Cell Rep.* **8,** 1583–1594 (2014).
5. Wojcechowskyj, J. A. *et al.* Quantitative phosphoproteomics reveals extensive cellular reprogramming during HIV-1 entry. *Cell Host Microbe* **13,** 613–623 (2013).
6. Kato, A. *et al.* Herpes simplex virus 1 protein kinase Us3 phosphorylates viral dUTPase and regulates its catalytic activity in infected cells. *J. Virol.* **88,** 655–666 (2014).
7. Humphrey, S. J., Azimifar, S. B. & Mann, M. High-throughput phosphoproteomics reveals in vivo insulin signaling dynamics. *Nat. Biotechnol.* (2015). doi:10.1038/nbt.3327
8. Moss, B. Poxviridae: the viruses and their replication. in *Fields virology* (eds. Estes, M. K., Kapikian, A. Z. & Knipe, D. M.) (Lippincott Williams & Wilkins, Philadelphia (2007), 2007).
9. Resch, W., Hixson, K. K., Moore, R. J., Lipton, M. S. & Moss, B. Protein composition of the vaccinia virus mature virion. *Virology* **358,** 233–247 (2007).
10. Chung, C.-S. *et al.* Vaccinia virus proteome: identification of proteins in vaccinia virus intracellular mature virion particles. *J. Virol.* **80,** 2127–2140 (2006).
11. Condit, R. C., Moussatche, N. & Traktman, P. In a nutshell: structure and assembly of the vaccinia virion. *Adv. Virus Res.* **66,** 31–124 (2006).
12. Lin, S. & Broyles, S. S. Vaccinia protein kinase 2: a second essential serine/threonine protein kinase encoded by vaccinia virus. *Proc. Natl. Acad. Sci. U. S. A.* **91,** 7653–7657 (1994).
13. Wang, S. & Shuman, S. Vaccinia virus morphogenesis is blocked by temperature-sensitive mutations in the F10 gene, which encodes protein kinase 2. *J. Virol.* **69,**

6376–6388 (1995).

14. Byrd, C. M., Bolken, T. C. & Hruby, D. E. The vaccinia virus I7L gene product is the core protein proteinase. *J. Virol.* **76,** 8973–8976 (2002).
15. Ericsson, M. *et al.* Characterization of ts 16, a temperature-sensitive mutant of vaccinia virus. *J. Virol.* **69,** 7072–7086 (1995).
16. Traktman, P., Caligiuri, A., Jesty, S. A., Liu, K. & Sankar, U. Temperature-sensitive mutants with lesions in the vaccinia virus F10 kinase undergo arrest at the earliest stage of virion morphogenesis. *J. Virol.* **69,** 6581–6587 (1995).
17. Hedengren-Olcott, M., Byrd, C. M., Watson, J. & Hruby, D. E. The vaccinia virus G1L putative metalloproteinase is essential for viral replication in vivo. *J. Virol.* **78,** 9947–9953 (2004).
18. Ansarah-Sobrinho, C. & Moss, B. Role of the I7 protein in proteolytic processing of vaccinia virus membrane and core components. *J. Virol.* **78,** 6335–6343 (2004).
19. Ansarah-Sobrinho, C. & Moss, B. Vaccinia virus G1 protein, a predicted metalloprotease, is essential for morphogenesis of infectious virions but not for cleavage of major core proteins. *J. Virol.* **78,** 6855–6863 (2004).
20. Senkevich, T. G., White, C. L., Koonin, E. V. & Moss, B. Complete pathway for protein disulfide bond formation encoded by poxviruses. *Proc. Natl. Acad. Sci. U. S. A.* **99,** 6667–6672 (2002).
21. Guan, K. L., Broyles, S. S. & Dixon, J. E. A Tyr/Ser protein phosphatase encoded by vaccinia virus. *Nature* **350,** 359–362 (1991).
22. Liu, K., Lemon, B. & Traktman, P. The dual-specificity phosphatase encoded by vaccinia virus, VH1, is essential for viral transcription in vivo and in vitro. *J. Virol.* **69,** 7823–7834 (1995).
23. Mercer, J. & Traktman, P. Genetic and cell biological characterization of the

vaccinia virus A30 and G7 phosphoproteins. *J. Virol.* **79,** 7146–7161 (2005).

24. Derrien, M., Punjabi, A., Khanna, M., Grubisha, O. & Traktman, P. Tyrosine Phosphorylation of A17 during Vaccinia Virus Infection: Involvement of the H1 Phosphatase and the F10 Kinase. *J. Virol.* **73,** 7287–7296 (1999).
25. Betakova, T., Wolffe, E. J. & Moss, B. Regulation of vaccinia virus morphogenesis: phosphorylation of the A14L and A17L membrane proteins and C-terminal truncation of the A17L protein are dependent on the F10L kinase. *J. Virol.* **73,** 3534–3543 (1999).
26. Szajner, P., Weisberg, A. S. & Moss, B. Evidence for an essential catalytic role of the F10 protein kinase in vaccinia virus morphogenesis. *J. Virol.* **78,** 257–265 (2004).
27. Assarsson, E. *et al.* Kinetic analysis of a complete poxvirus transcriptome reveals an immediate-early class of genes. *Proc. Natl. Acad. Sci. U. S. A.* **105,** 2140–2145 (2008).
28. Traktman, P. *et al.* Elucidating the essential role of the A14 phosphoprotein in vaccinia virus morphogenesis: construction and characterization of a tetracycline-inducible recombinant. *J. Virol.* **74,** 3682–3695 (2000).
29. Mercer, J. & Traktman, P. Investigation of structural and functional motifs within the vaccinia virus A14 phosphoprotein, an essential component of the virion membrane. *J. Virol.* **77,** 8857–8871 (2003).
30. Wu, Y. *et al.* Multilayered Genetic and Omics Dissection of Mitochondrial Activity in a Mouse Reference Population. *Cell* **158,** 1415–1430 (2014).
31. Ulaeto, D., Grosenbach, D. & Hruby, D. E. The vaccinia virus 4c and A-type inclusion proteins are specific markers for the intracellular mature virus particle. *J. Virol.* **70,** 3372–3377 (1996).

32. Matson, J., Chou, W., Ngo, T. & Gershon, P. D. Static and dynamic protein phosphorylation in the Vaccinia virion. *Virology* **452-453,** 310–323 (2014).
33. Byrd, C. M., Bolken, T. C. & Hruby, D. E. Molecular dissection of the vaccinia virus I7L core protein proteinase. *J. Virol.* **77,** 11279–11283 (2003).
34. Condit, R. C., Motyczka, A. & Spizz, G. Isolation, characterization, and physical mapping of temperature-sensitive mutants of vaccinia virus. *Virology* **128,** 429–443 (1983).
35. Pengue, G., Caputo, A., Rossi, C., Barbanti-Brodano, G. & Lania, L. Transcriptional silencing of human immunodeficiency virus type 1 long terminal repeat-driven gene expression by the Krüppel-associated box repressor domain targeted to the transactivating response element. *J. Virol.* **69,** 6577–6580 (1995).
36. Punjabi, A. & Traktman, P. Cell biological and functional characterization of the vaccinia virus F10 kinase: implications for the mechanism of virion morphogenesis. *J. Virol.* **79,** 2171–2190 (2005).
37. Grimley, P. M., Rosenblum, E. N., Mims, S. J. & Moss, B. Interruption by Rifampin of an early stage in vaccinia virus morphogenesis: accumulation of membranes which are precursors of virus envelopes. *J. Virol.* **6,** 519–533 (1970).
38. Unger, B. & Traktman, P. Vaccinia virus morphogenesis: a13 phosphoprotein is required for assembly of mature virions. *J. Virol.* **78,** 8885–8901 (2004).
39. Rodriguez, D., Rodriguez, J. R. & Esteban, M. The vaccinia virus 14-kilodalton fusion protein forms a stable complex with the processed protein encoded by the vaccinia virus A17L gene. *J. Virol.* **67,** 3435–3440 (1993).
40. Vanslyke, J. K., Whitehead, S. S., Wilson, E. M. & Hruby, D. E. The multistep proteolytic maturation pathway utilized by vaccinia virus P4a protein: a degenerate conserved cleavage motif within core proteins. *Virology* **183,** 467–478 (1991).

41. Sarov, I. & Joklik, W. K. Studies on the nature and location of the capsid polypeptides of vaccinia virions. *Virology* **50,** 579–592 (1972).
42. VanSlyke, J. K., Franke, C. A. & Hruby, D. E. Proteolytic maturation of vaccinia virus core proteins: identification of a conserved motif at the N termini of the 4b and 25K virion proteins. *J. Gen. Virol.* **72 (Pt 2),** 411–416 (1991).
43. Whitehead, S. S. & Hruby, D. E. Differential utilization of a conserved motif for the proteolytic maturation of vaccinia virus proteins. *Virology* **200,** 154–161 (1994).
44. Yang, W. P., Kao, S. Y. & Bauer, W. R. Biosynthesis and post-translational cleavage of vaccinia virus structural protein VP8. *Virology* **167,** 585–590 (1988).
45. Bisht, H., Weisberg, A. S., Szajner, P. & Moss, B. Assembly and disassembly of the capsid-like external scaffold of immature virions during vaccinia virus morphogenesis. *J. Virol.* **83,** 9140–9150 (2009).
46. Szajner, P., Weisberg, A. S., Lebowitz, J., Heuser, J. & Moss, B. External scaffold of spherical immature poxvirus particles is made of protein trimers, forming a honeycomb lattice. *J. Cell Biol.* **170,** 971–981 (2005).
47. Unger, B., Mercer, J., Boyle, K. A. & Traktman, P. Biogenesis of the vaccinia virus membrane: genetic and ultrastructural analysis of the contributions of the A14 and A17 proteins. *J. Virol.* **87,** 1083–1097 (2013).
48. Gross, C. H. & Shuman, S. Vaccinia virions lacking the RNA helicase nucleoside triphosphate phosphohydrolase II are defective in early transcription. *J. Virol.* **70,** 8549–8557 (1996).
49. Broyles, S. S., Yuen, L., Shuman, S. & Moss, B. Purification of a factor required for transcription of vaccinia virus early genes. *J. Biol. Chem.* **263,** 10754–10760 (1988).
50. Hu, X., Wolffe, E. J., Weisberg, A. S., Carroll, L. J. & Moss, B. Repression of the A8L gene, encoding the early transcription factor 82-kilodalton subunit, inhibits

morphogenesis of vaccinia virions. *J. Virol.* **72,** 104–112 (1998).

51. Resch, W. & Moss, B. The conserved poxvirus L3 virion protein is required for transcription of vaccinia virus early genes. *J. Virol.* **79,** 14719–14729 (2005).
52. Yang, Z. & Moss, B. Interaction of the vaccinia virus RNA polymerase-associated 94-kilodalton protein with the early transcription factor. *J. Virol.* **83,** 12018–12026 (2009).
53. Hagen, C. J., Titong, A., Sarnoski, E. A. & Verardi, P. H. Antibiotic-dependent expression of early transcription factor subunits leads to stringent control of vaccinia virus replication. *Virus Res.* **181,** 43–52 (2014).
54. Hu, X., Carroll, L. J., Wolffe, E. J. & Moss, B. De novo synthesis of the early transcription factor 70-kilodalton subunit is required for morphogenesis of vaccinia virions. *J. Virol.* **70,** 7669–7677 (1996).
55. Manning, G., Whyte, D. B., Martinez, R., Hunter, T. & Sudarsanam, S. The protein kinase complement of the human genome. *Science* **298,** 1912–1934 (2002).
56. Duan, G., Li, X. & Köhn, M. The human DEPhOsphorylation database DEPOD: a 2015 update. *Nucleic Acids Res.* **43,** D531–5 (2015).
57. Hutchinson, E. C. *et al.* Mapping the phosphoproteome of influenza A and B viruses by mass spectrometry. *PLoS Pathog.* **8,** e1002993 (2012).
58. Bergström Lind, S. *et al.* The phosphoproteome of the adenovirus type 2 virion. *Virology* **433,** 253–261 (2012).
59. Ngo, T., Mirzakhanyan, Y., Moussatche, N. & Gershon, P. D. Protein primary structure of the Vaccinia virion at increased resolution. *J. Virol.* (2016). doi:10.1128/JVI.01042-16
60. Bidgood, S. R. & Mercer, J. Cloak and Dagger: Alternative Immune Evasion and Modulation Strategies of Poxviruses. *Viruses* **7,** 4800–4825 (2015).

61. Schmidt, F. I., Bleck, C. K. E., Helenius, A. & Mercer, J. Vaccinia extracellular virions enter cells by macropinocytosis and acid-activated membrane rupture. *EMBO J.* **30,** 3647–3661 (2011).
62. Schmidt, F. I. *et al.* Vaccinia virus entry is followed by core activation and proteasome-mediated release of the immunomodulatory effector VH1 from lateral bodies. *Cell Rep.* **4,** 464–476 (2013).
63. Kilcher, S. *et al.* siRNA screen of early poxvirus genes identifies the AAA+ ATPase D5 as the virus genome-uncoating factor. *Cell Host Microbe* **15,** 103–112 (2014).
64. Mercer, J. & Helenius, A. Vaccinia virus uses macropinocytosis and apoptotic mimicry to enter host cells. *Science* **320,** 531–535 (2008).
65. Bodenmiller, B. & Aebersold, R. Quantitative analysis of protein phosphorylation on a system-wide scale by mass spectrometry-based proteomics. *Methods Enzymol.* **470,** 317–334 (2010).
66. Eng, J. K., McCormack, A. L. & Yates, J. R. An approach to correlate tandem mass spectral data of peptides with amino acid sequences in a protein database. *J. Am. Soc. Mass Spectrom.* **5,** 976–989 (1994).
67. Keller, A., Nesvizhskii, A. I., Kolker, E. & Aebersold, R. Empirical statistical model to estimate the accuracy of peptide identifications made by MS/MS and database search. *Anal. Chem.* **74,** 5383–5392 (2002).
68. Choi, M. *et al.* MSstats: an R package for statistical analysis of quantitative mass spectrometry-based proteomic experiments. *Bioinformatics* **30,** 2524–2526 (2014).
69. Benjamini, Y. & Hochberg, Y. Controlling the False Discovery Rate: A Practical and Powerful Approach to Multiple Testing. *J. R. Stat. Soc. Series B Stat. Methodol.* **57,** 289–300 (1995).
70. UniProt Consortium. UniProt: a hub for protein information. *Nucleic Acids Res.* **43,**

D204–12 (2015).

71. Shteynberg, D. *et al.* PTMProphet: TPP Software for Validation of Modified Site Locations on Post-Translationally Modified Peptides. in *60th American Society for Mass Spectrometry (ASMS) Annual Conference* (2012).
72. Schilling, B. *et al.* Platform-independent and label-free quantitation of proteomic data using MS1 extracted ion chromatograms in skyline: application to protein acetylation and phosphorylation. *Mol. Cell. Proteomics* **11,** 202–214 (2012).
73. Bruderer, R. *et al.* Extending the limits of quantitative proteome profiling with data-independent acquisition and application to acetaminophen treated 3D liver microtissues. *Mol. Cell. Proteomics* (2015). doi:10.1074/mcp.M114.044305
74. Bruderer, R. *et al.* Optimization of Experimental Parameters in Data-Independent Mass Spectrometry Significantly Increases Depth and Reproducibility of Results. *Mol. Cell. Proteomics* **16,** 2296–2309 (2017).
75. Cox, J. & Mann, M. MaxQuant enables high peptide identification rates, individualized ppb-range mass accuracies and proteome-wide protein quantification. *Nat. Biotechnol.* (2008).
76. Cox, J. *et al.* Andromeda: a peptide search engine integrated into the MaxQuant environment. *J. Proteome Res.* **10,** 1794–1805 (2011).
77. Roland Bruderer, Lynn Verbeke, Oliver M. Bernhardt, Tejas Gandhi, Jan Muntel, Yue Xuan, Lukas Reiter. Spectral library-free DIA (DDA-free DIA) algorithm applied to data generated on a novel fast scanning Orbitrap instrument. (4-8 June 2017).
78. Fathi, Z. & Condit, R. C. Phenotypic characterization of a vaccinia virus temperature-sensitive complementation group affecting a virion component. *Virology* **181,** 273–276 (1991).

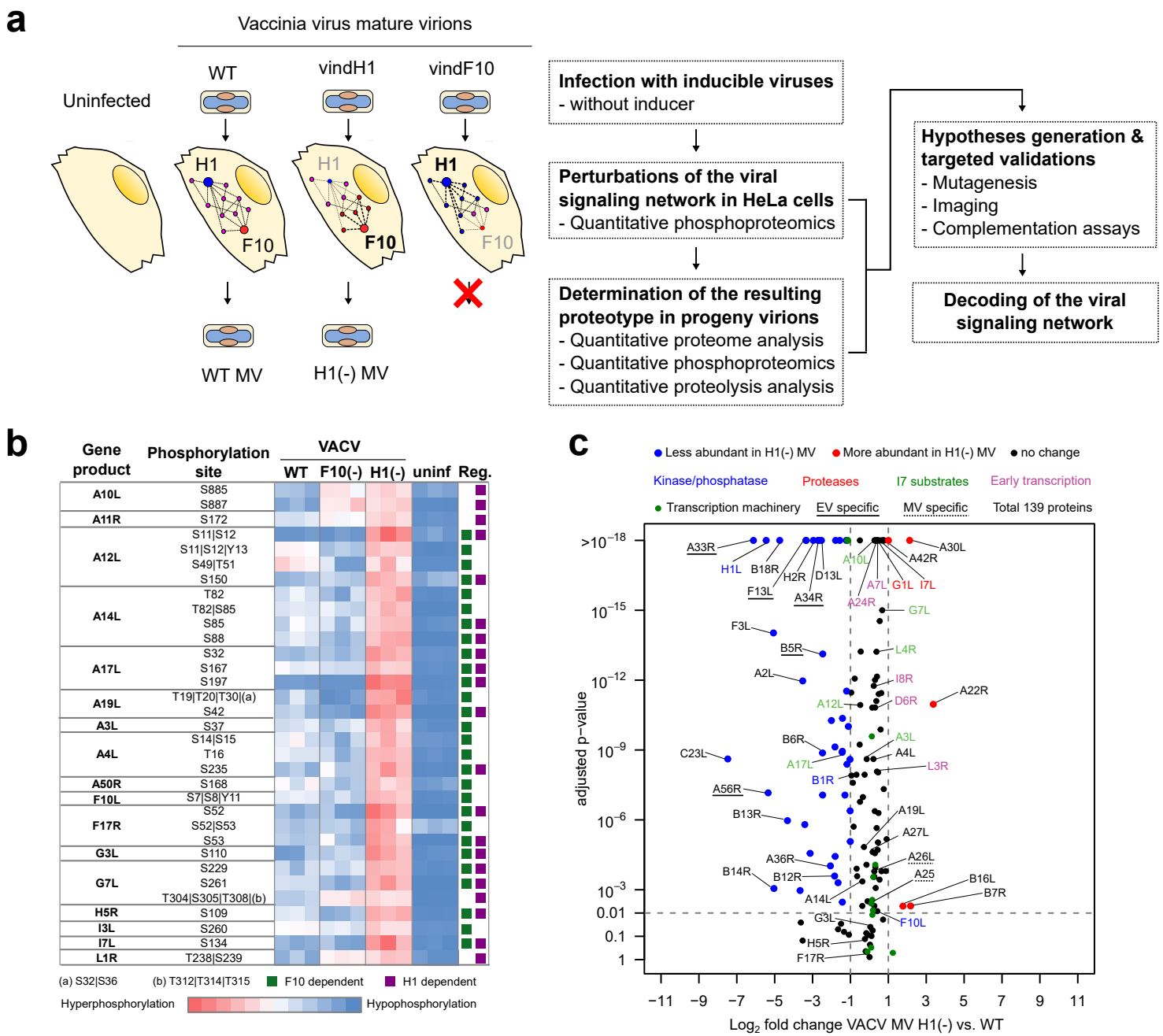

Novy & Kilcher Figure 1

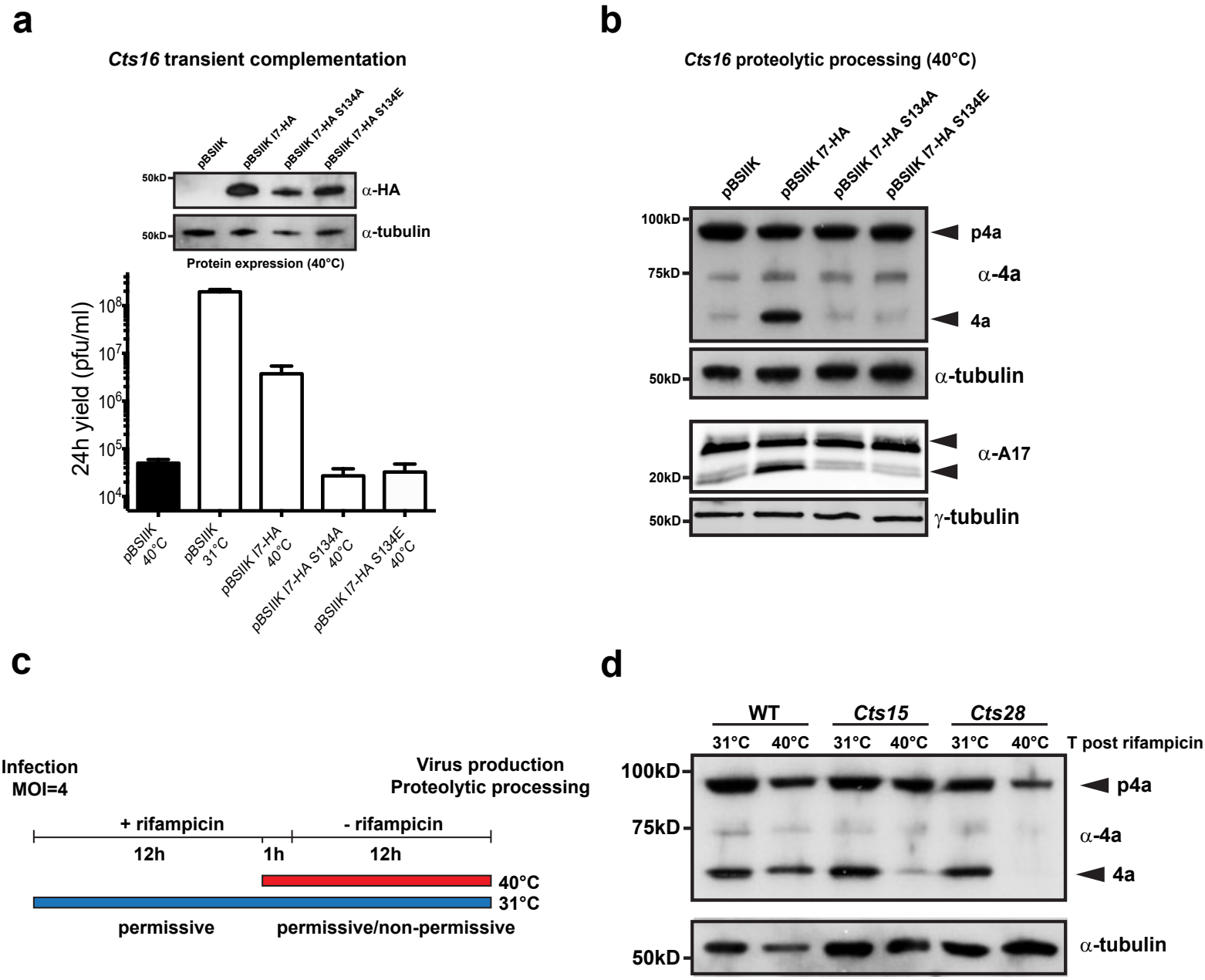

Novy & Kilcher Figure 2

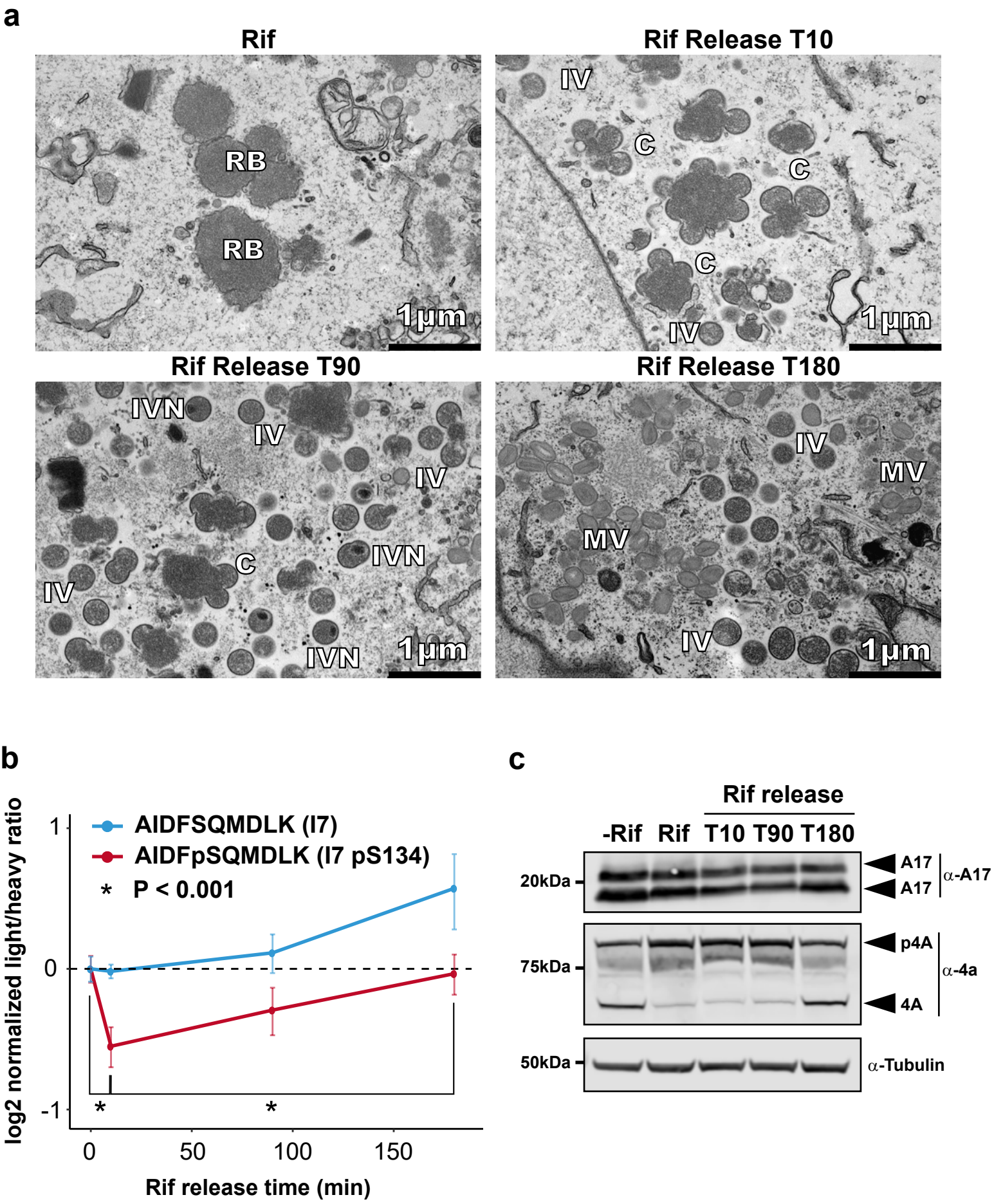

Novy & Kilcher Figure 3

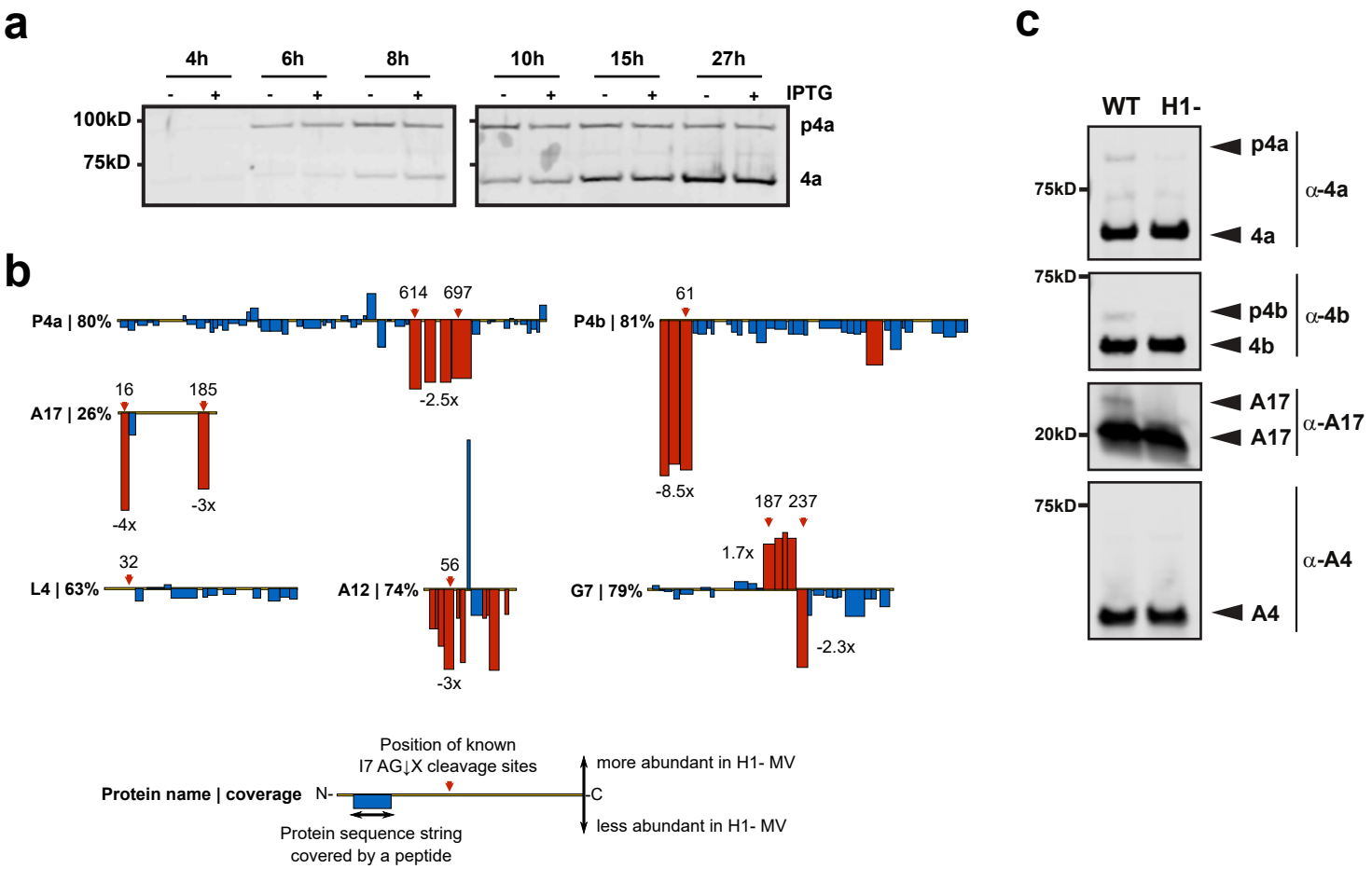

Novy & Kilcher Figure 4

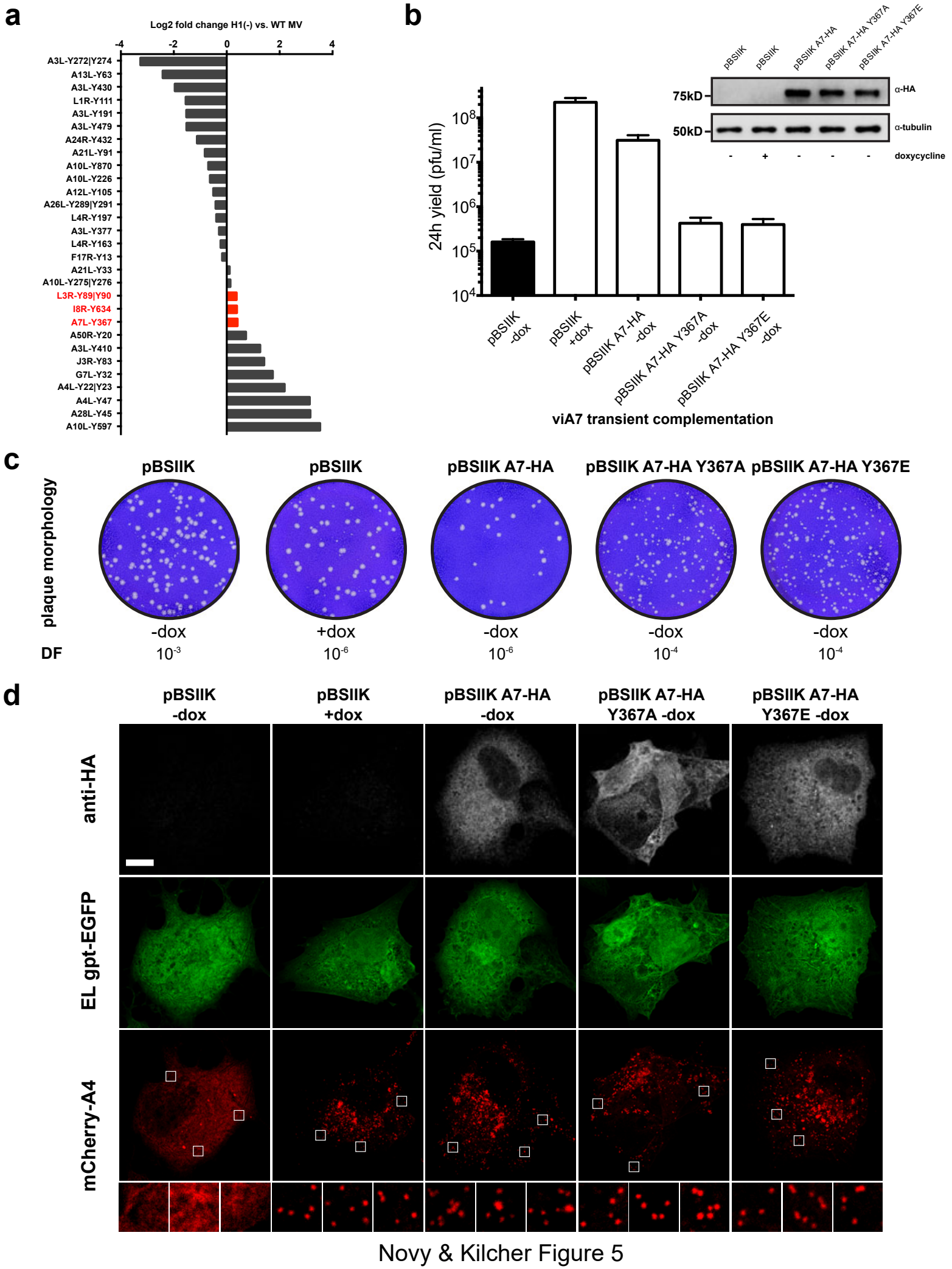

Novy & Kilcher Figure 5

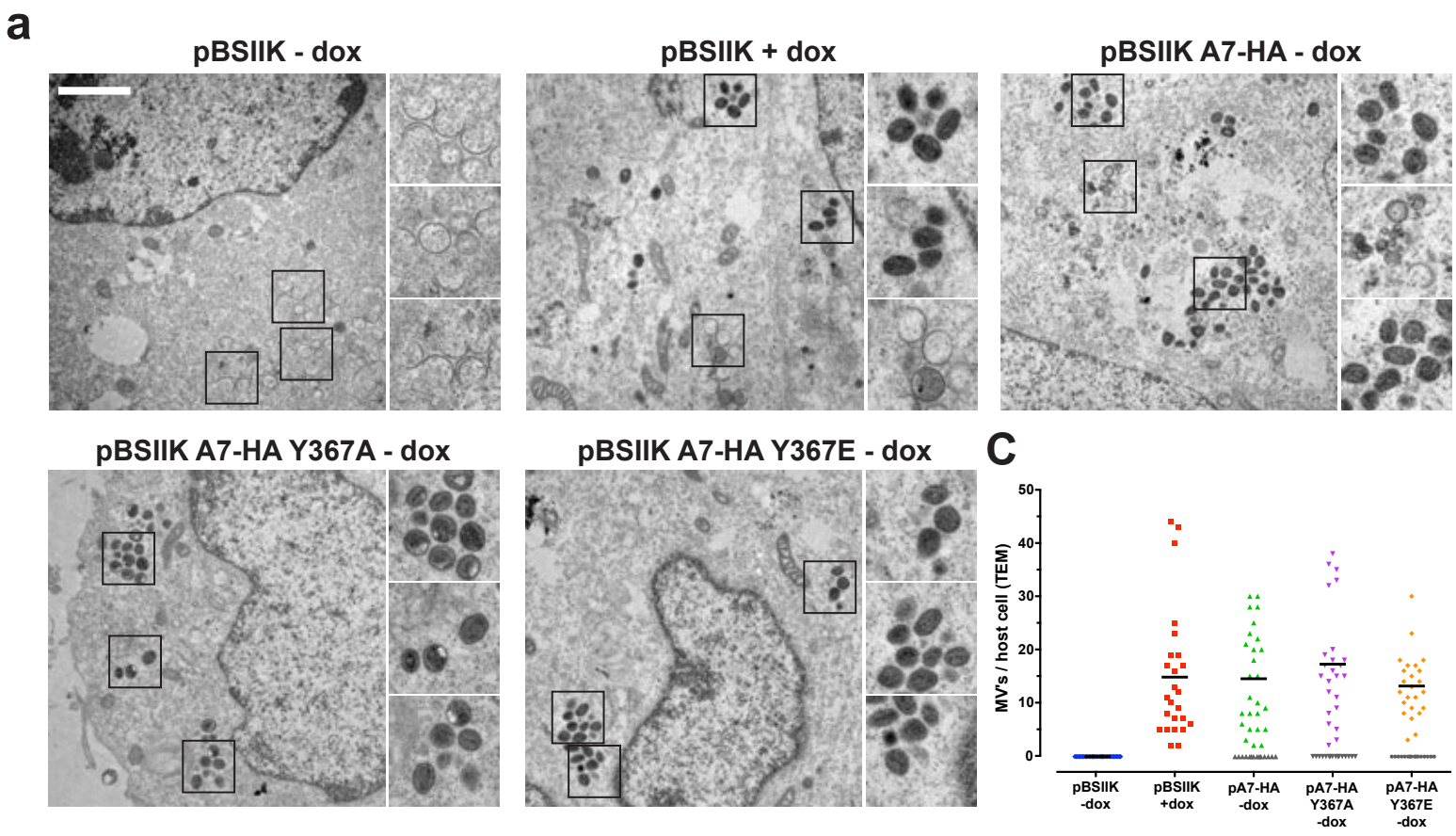

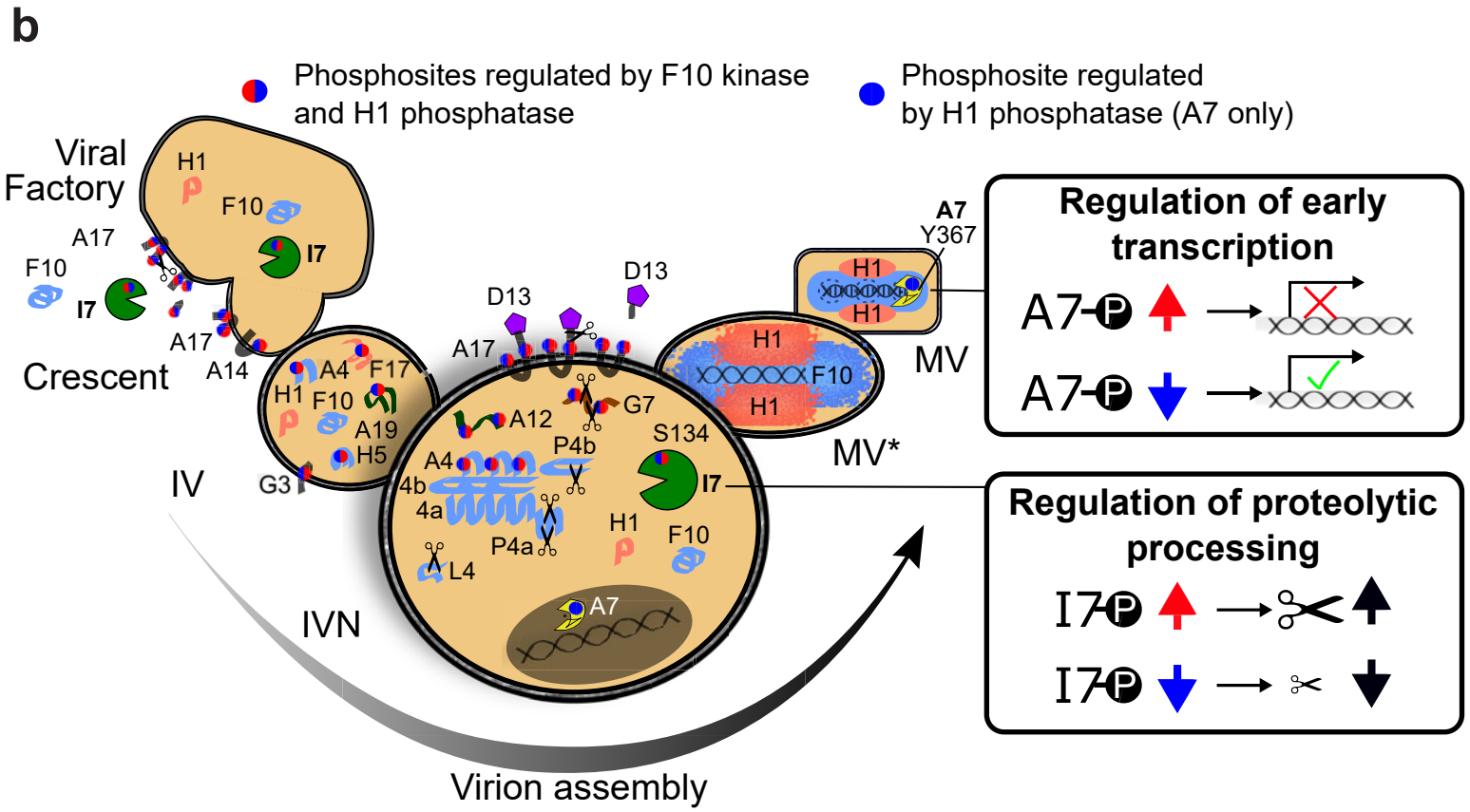

Novy & Kilcher Figure 6